Original Research

Reconstruction of the Human Visual System Based on DTI Fiber Tracking

Philipp Staempfli, PhD,[1,2]* Anna Rienmueller, MD,[1] Carolin Reischauer, MSc,[1] Anton Valavanis, MD,[2] Peter Boesiger, PhD,[1] and Spyridon Kollias, MD[2]

Purpose: To apply and to evaluate the newly developed advanced fast marching algorithm (aFM) in vivo by reconstructing the human visual pathway, which is characterized by areas of extensive fiber crossing and branching, i.e., the optic chiasm and the lateral geniculate nucleus (LGN).

Materials and Methods: Diffusion tensor images were acquired in 10 healthy volunteers. Due to the proximity to bony structures and air-filled spaces of the optic chiasm, a high sensitivity encoding (SENSE) reduction factor was applied to reduce image distortions in this area. To reconstruct the visual system, three different seed areas were chosen separately. The results obtained by the aFM tracking algorithm were compared and validated with known anatomy.

Results: The visual system could be reconstructed reproducibly in all subjects and the reconstructed fiber pathways are in good agreement with known anatomy.

Conclusion: The present work shows that the advanced aFM, which is especially designed for overcoming tracking limitations within areas of extensive fiber crossing, handles the fiber crossing and branching within the optic chiasm and the LGN correctly, thus allowing the reconstruction of the entire human visual fiber pathway, from the intraorbital segment of the optic nerves to the visual cortex.

Key Words: diffusion tensor tractography; resolving fiber crossing; visual system; DTI; fast marching
J. Magn. Reson. Imaging 2007;26:886–893.

DIFFUSION TENSOR IMAGING (DTI) (1,2) and its application, DTI fiber tractography (3–5), has become a prominent tool for mapping white matter axonal structures and investigating their structural integrity in the human brain since its introduction a decade ago. For fiber tracking, a variety of different tracking algorithms has been proposed so far (for review articles, see Refs. 6 and 7). Despite the promising applications of DTI fiber tracking in brain research and clinical studies, this technique is still constricted by several limitations. A severe drawback is the tensor's voxel-averaged nature, i.e., the principal eigenvector does not necessarily correspond to the main fiber direction, particularly when bundles intersect, branch, or merge. For whole-brain DTI fiber tracking, the voxel size of the data that can be achieved in a clinically feasible acquisition time is approximately 1.5 mm^3. This is orders of magnitudes larger than the diameter of a single axon, which lies in the range of a few microns. Therefore, only major fiber bundles can be resolved, and it is not possible to trace the course of single axons with DTI. But even when main fiber systems are investigated, trajectories may be compromised by missing or wrong directional information in the main diffusion eigenvector due to noise, partial volume effects, or, likewise, fiber crossing, branching, or kissing situations (8–14). Sophisticated tracking algorithms have been developed recently to overcome these limitations and to improve the tracking results, e.g., by allowing fiber branching or by resolving fiber crossing situations (15–20).

Another limitation in the field of DTI fiber tracking is the lack of standardized procedures for verifying or quantifying DTI revealed connections, which makes it difficult to compare tracking results of different algorithms with each other. Anatomical variations between subjects (21–24) and missing knowledge of the exact course of fiber connections beyond the gross fiber pathways further complicate in vivo fiber tracking evaluations. Several bundles of these main fiber connections, such as, e.g., the corpus callosum, superior, anterior, and posterior thalamic radiations, inferior and superior longitudinal fasciculi, inferior frontooccipital tract, and sagittal stratum, were reconstructed in the last few years. A summary can be found in a 3D in vivo atlas by Mori et al (25) and a publication by Wakana et al (26).

An anatomically well known fiber system investigated with DTI fiber tracking is the human visual pathway. Trip et al (27) and Iwasawa et al (28) investigated the optic nerves in patients suffering from optic neuritis. A study (29) on the same disease showed pathologic changes in the optic radiation on maps generated with the fast marching tracking technique (19). Schoth et al

[1]Institute for Biomedical Engineering, Swiss Federal Institute of Technology (ETH) Zurich and University Zurich, Zurich, Switzerland.
[2]Institute of Neuroradiology, University Hospital Zurich, Zurich, Switzerland.
*Address reprint requests to: P.S., Institute for Biomedical Engineering, University and ETH Zurich, Gloriastrasse 35, CH - 8092 Zurich, Switzerland. E-mail: staempfli@biomed.ee.ethz,ch
Received November 7, 2006; Accepted July 3, 2007.
DOI 10.1002/jmri.21098
Published online in Wiley InterScience (www.interscience.wiley.com).

(30) explored the optic radiation in blind humans and in healthy volunteers and compared anisotropy values between the two groups. Different MR techniques to acquire images of the optic nerve, the optic chiasm, and the optic tract have been investigated by Vinogradov et al (31). DTI fiber tracking reconstructions of the optic radiation in healthy volunteers are presented in Parker et al (19) and Staempfli et al (20). Until now, there exists no study attempting to reconstruct the entire visual pathway using DTI data. The main reasons for that are susceptibility artifacts in the area of the chiasm as well as the extensive fiber crossing within this area, which is difficult to resolve by fiber tracking algorithms.

The goal of this study was to reconstruct the entire human visual pathway, from the optic nerve to the visual cortex, using a single tracking seed area, which has not been achieved until now. Therefore, the newly developed advanced fast marching algorithm (aFM) (20) was applied and its results were compared and analyzed to known anatomy. A main focus was to explore the performance of the algorithm in the area of the optic chiasm. Particularly, the hypothesis being tested was whether the aFM algorithm, which was especially designed for resolving fiber crossings, is capable of resolving this anatomically challenging situation in the human visual pathway.

The Human Visual System and the Visual Pathway

In this paragraph, a short summary is provided about the anatomy of the most important structures of the human visual system. More detailed anatomical insights can be found, e.g., in Standring (32). The human visual system is subdivided into several parts (see Fig. 1). The retina (Fig. 1a), the sensory input organ of the visual system, transmits neural impulses through the optic nerve (Fig. 1b) to the optic chiasm (Fig. 1c), which is positioned at the chiasmatic sulcus in the skull base, at the junction of the anterior wall and the floor of the third ventricle. From there, fibers of the optic nerves diverge into medial and lateral hemiparts, where medial parts are crossing to the contralateral side and lateral parts continue on the ipsilateral side of the brain within the optic tract (Fig. 1d). The main part of the fibers of the optic tract terminates in the lateral geniculate nucleus (LGN) (Fig. 1e). Only a few fibers pass on to the superior colliculus (Fig. 1f). A main efferent fiber connection from the LGN passes on via the optic radiation (Fig. 1g) and terminates in the visual cortex (Fig. 1h). Thereby, fibers first turn laterally and pass through the sublenticular part of the internal capsule before running backward through the external sagittal stratum of the temporal and occipital lobes, ending within the striate cortex (32,33).

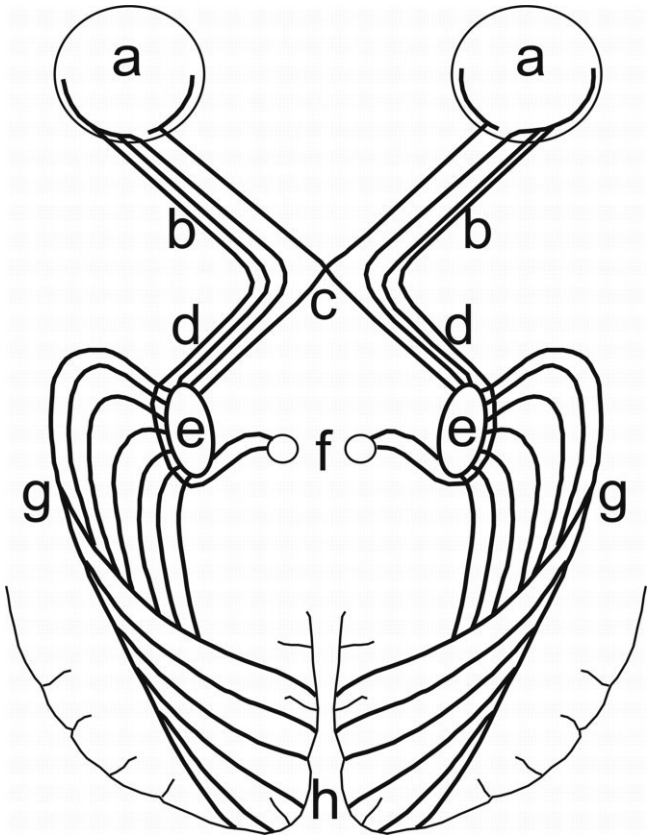

Figure 1. Schematic depiction of the human visual system and the visual pathway: (**a**) eyes with eyeball and retina, (**b**) optic nerves, (**c**) optic chiasm, (**d**) optic tracts, (**e**) lateral geniculate nuclei (LGN), (**f**) superior colliculi, (**g**) optic radiations, and (**h**) visual cortex.

MATERIALS AND METHODS

Subjects and Data Acquisition

A total of eight healthy volunteers (mean age 24.7 ± 5.0 years, five female, three male) were scanned. Four of them were scanned twice in different sessions to test the intrareproducibility of our results. Each subject gave informed, written consent before the study. All acquisitions were performed using a 3 T Achieva whole-body system (Philips Medical Systems, Best, the Netherlands), equipped with 80 mT/m/msec gradient coils and an eight-element receive head coil array (MRI Devices Corp., Waukesha, WI, USA). To minimize head motion, the subjects were fixed in the head coil by using foam padding. Additionally, they were asked to close their eyes during the acquisition to reduce eye movements.

All sessions consisted of one high-resolution T1-weighted anatomical scan and two DTI scans with different cardiac gating times, to investigate whether fiber tracking results within the optic system are compromised by pulsation and motion effects. The total scan time, including survey and sensitivity encoding (SENSE) reference scan, added up to approximately 55 minutes. The anatomical data were obtained in a T1-weighted turbo field echo (TFE) scan consisting of 27 contiguous slices (field of view [FOV] = 220 × 220 mm^2, slice thickness = 0.6 mm, acquisition matrix size = 256 × 256 mm^2, TR = 20 ms, $\alpha = 20°$). For the DTI scans, a diffusion-weighted single-shot spin-echo echo planar imaging (EPI) sequence was applied (FOV = 220 × 220 mm^2, acquisition matrix size = 96 × 96,

reconstructed to 128 × 128, contiguous slices =9, slice thickness = 1.8 mm, TE = 45.8 msec, number of signal averages = 7, partial Fourier acquisition = 60%). Diffusion weighting with a maximal b-factor of 1000 seconds/mm^2 was carried out along 15 icosahedral directions (34), complemented by one scan with b = 0. To reduce susceptibility artifacts and to enhance signal-to-noise ratio (SNR) and image quality (35–37), SENSE (38) with a reduction factor R = 5 was applied. To further reduce pulsation and flow artifacts (39,40) and improve fiber tracking results (41,42), cardiac gating was applied for the DTI acquisition using electrocardiography (ECG). Image acquisition was started at two different time points, namely 200 msec and 300 msec from the monitored R wave.

Data Preprocessing

Retrospective interscan motion corrections and a decrease of eddy current–induced image warping were achieved using a correlation-based 3D-affine registration algorithm (43). Moreover, the anatomical T1 images were coregistered to the DTI data with SPM2 (SPM2; Wellcome Department of Cognitive Neurology, London, UK), whereas the BO-image was used as target image. All further calculations, such as determining the independent elements of the diffusion tensor, deriving the corresponding eigenvalues and eigenvectors, and reconstructing fibers, were performed with a dedicated software package developed in C++.

Fiber Reconstruction

The different seed regions for the fiber tracking algorithm were selected on the coregistered T1 images that were overlaid on the DTI data. All seed areas were defined on transversal slices. As first start region, an area consisting of four to eight voxels, depending on the individual anatomy, was chosen in the center of the optic chiasm (Fig. 2). Therewith, fibers emerging from the optic chiasm into the two optic nerves and into the two optic tracts were investigated. As second and third seed area, voxels in the intraorbital portion of the left and right optic nerves, respectively, were defined (Fig. 2). For all fiber reconstructions, the aFM (20) algorithm was applied. In contrast to conventional line propagation algorithms, such as, e.g., the well established "fiber assignment by continuous tracking" (FACT) algorithm (7), fast marching techniques are based on evolving a 3D wave front through a volume of interest (19,44). The rate at which the front expands is linked to the local diffusion tensor and its orientation to adjacent diffusion tensors. Until today, all proposed FM algorithms incorporate only the principal eigenvector of the diffusion tensor in their calculations. Therefore, these methods fail to reconstruct fiber tracks in crossing or kissing areas. The newly developed aFM algorithm proposed an advanced implementation of FM, combining the advantages of classical FM and the tensor deflection approach (15). The aFM algorithm takes into account the entire information contained in the diffusion tensor. Thereby, every tensor is classified as prolate (linear), oblate (planar), or spherical ellipsoid (17,45). During the actual tracking process, different adapted speed functions are applied for the front propagation, according to the shape classification of two adjacent voxels. As a result, the aFM algorithm features the capability to accurately evaluate brain areas containing fiber crossings and branching.

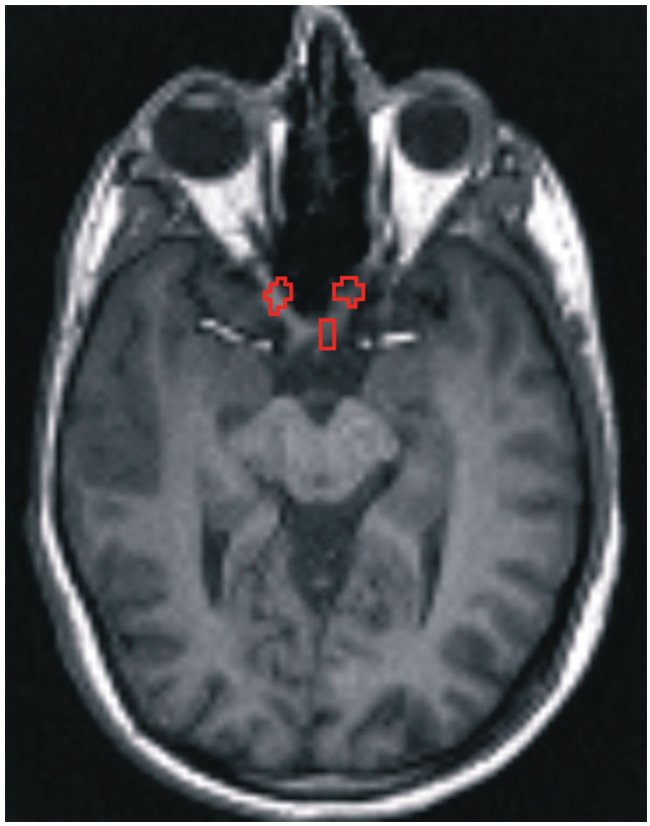

Figure 2. Selected seed regions on the coregistered T_1 images consisting of four to eight voxels, defined on transversal slices. One start region was chosen in the center of the optic chiasm, as the second and third seed area, voxels in the center of the left and right optic nerves, respectively, were defined. [Color figure can be viewed in the online issue, which is available at www.interscience.wiley.com]

In this study, the aFM algorithm was executed with 60,000 to 65,000 time steps. For reconstructing the fibers, an 8% to 12% voxel connectivity was used, depending on the subject's anatomy and size of the brain (20). One fiber reconstruction with these parameters took about 45 seconds on a standard PC.

Anatomical Evaluation

The resulting fiber pathways, reconstructed from the three above mentioned seed areas, were evaluated visually, whereas the main quality criteria were the integrity and the accuracy of the reconstructed fibers. Therefore, the course of the reconstructed fibers on the coregistered anatomical T1 data was compared with the known anatomy of the human visual pathway. Furthermore, the behavior of the algorithm in the region of the optic chiasm and the ability to resolve the fiber crossing within this complex structure was an important benchmark.

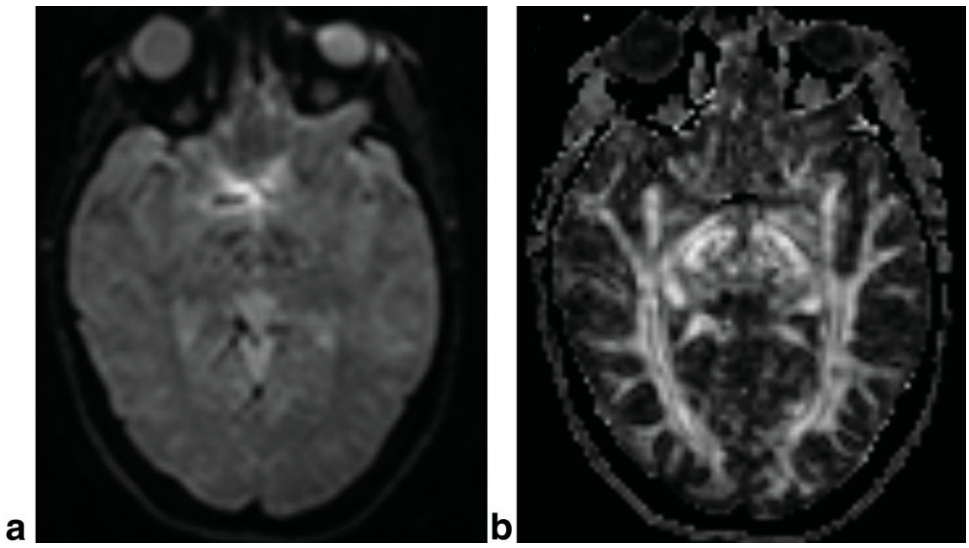

Figure 3. BO map (**a**) and corresponding FA map (**b**), which illustrate that the signal loss caused by the high sense factor could be adequately compensated by signal averaging.

RESULTS

Figure 3 shows exemplarily a BO image (Fig. 3a) and the corresponding fractional anisotropy (FA) image (Fig. 3b) of one subject. It emphasizes the high data quality that is not heavily compromised by noise. The SNR drop provoked by the high SENSE reduction factor (36,37) is adequately compensated by signal averaging during data acquisition (number of signal averages = 7). Figures 4 and 5 exemplify the reconstructed fibers for two of the eight different subjects for both cardiac trigger time points. Figure 4a and the first row in Fig. 5 show the data of one subject, acquired at the first cardiac trigger time point (200 msec). Figure 4b and the second row in Fig. 5 illustrate reconstructed fibers in the dataset of the second subject. Thereby, the data of the later cardiac gating time point (300 msec) were used. It is important to mention that reproducible fiber pathways were reconstructed in all other six subjects, and similar results were achieved in every volunteer dataset for both measured cardiac trigger time points.

In Fig. 4, fibers reconstructed from the center of the optic chiasm are shown. In both hemispheres of the brain, the optic nerve, the optic tract, and the connections to the LGN could be reconstructed bilaterally. Furthermore, fibers from the posterolateral thalamus continue to the optic radiation to reach the striate cortex in the occipital lobe. A few fibers emerging from the chiasm in posterior direction most probably represent

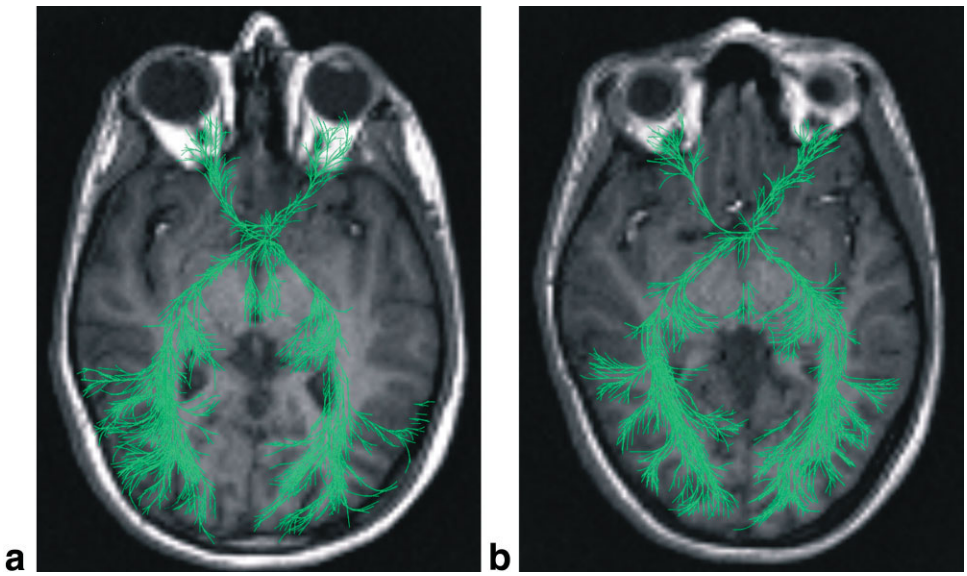

Figure 4. Fibers reconstructed from the center of the optic chiasm are shown. **a:** Data set of a subject, acquired at the cardiac trigger time point of 200 msec. **b:** Data set of a second subject at the cardiac gating time point of 300 msec. Trajectories calculated with the aFM algorithm are depicted in green. In both hemispheres of the brain, the optic nerve, the optic tract, the connections to the LGN, and furthermore the optic radiation onto the area striata in the occipital lobe, can be seen. The fibers emerging from the chiasm in the posterior direction most probably represent connections following the oculomotor nerve to its nuclei in the brain stem.

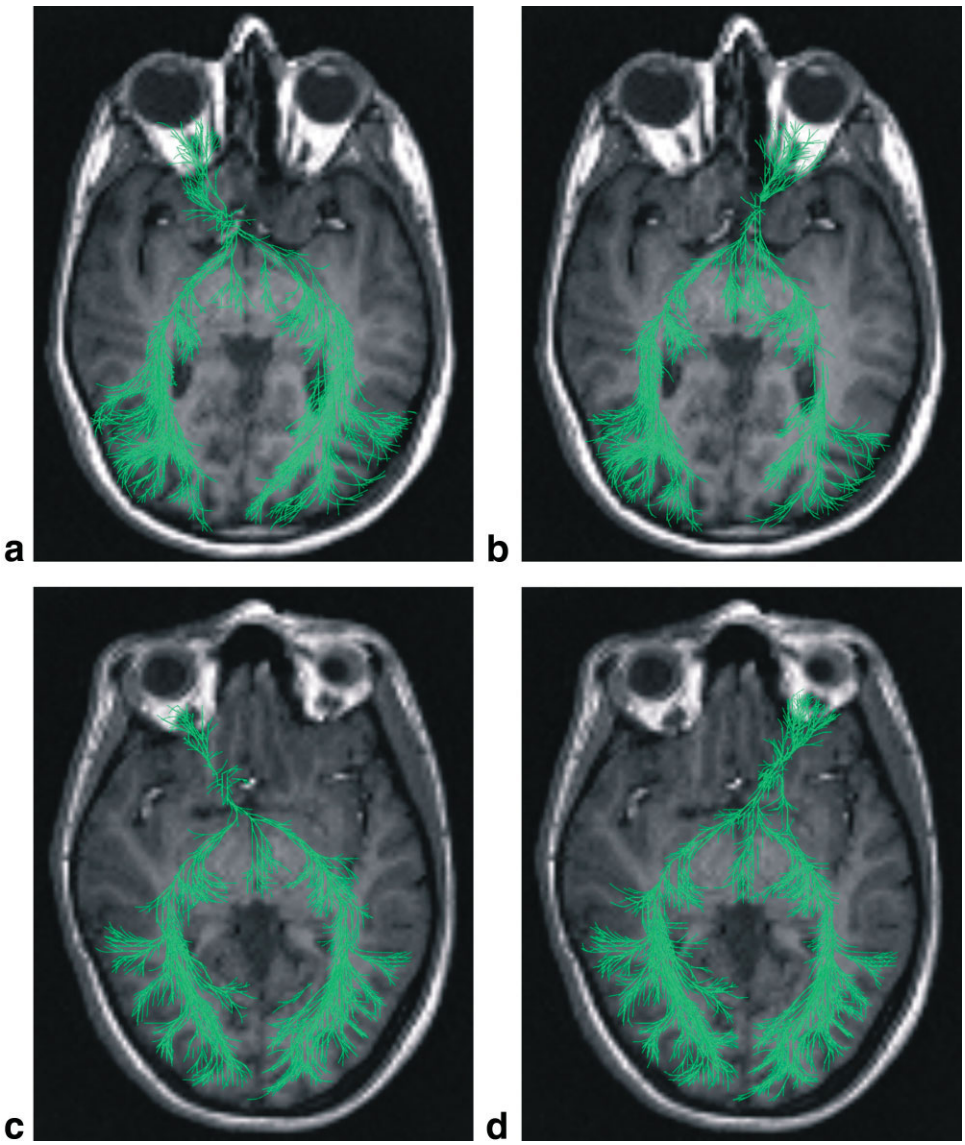

Figure 5. Trajectories, reconstructed from seed areas within the optic nerves. First row: data set of a subject, acquired at the cardiac trigger time point of 200 msec. Second row: data set of a second subject at the cardiac gating time point of 300 msec. The aFM-reconstructed fibers proceed from the seed region anterior in the direction of the retina and posterior to the chiasm, where they diverge into the left and right part of the optic tract and follow the optic radiations onto the visual cortex. Fibers are not deflected into the contralateral optic nerve and therefore it is not reconstructed by the aFM algorithm. Additional fibers starting from the chiasm directly in the posterior direction and fibers passing from the optic radiation into the posterior lateral parts of the cerebral cortex are almost congruent as in Fig. 4a and b, respectively.

connections following the oculomotor nerve to its nuclei in the brain stem.

Figure 5 illustrates the trajectories, reconstructed from seed areas encompassing the optic nerves. Proceeding from the seed region, the aFM algorithm reconstructs the optic nerve in both directions, anterior in the direction of the retina and posterior to the chiasm. The fibers diverge inside the chiasm into the left and right part of the optic tract and follow the optic radiations onto the visual cortex. As physiologically expected, fibers are not deflected into the contralateral optic nerve and, therefore, this is not reconstructed by the aFM algorithm. Additional fibers starting from the chiasm directly in posterior direction and fibers passing from the optic radiation into posterior lateral parts of the cerebral cortex are almost congruent, as in Fig. 4a and b, respectively.

DISCUSSION

The human visual system is a large, well characterized anatomical structure in the brain that has already been studied extensively in humans and primates. Performing fiber tracking based on DTI data within this fiber system still faces four main challenges:

First, the anatomical location of the optic chiasm is positioned in close proximity to the bony structures of the anterior and middle cranial fossa where several air filled spaces, the sinuses within the sphenoid and ethmoid bone, are located. These cavities are source of susceptibility-related artifacts during DTI data acquisition. A well-established approach to reduce these image distortions is the application of parallel imaging techniques, such as, e.g., SENSE. In this study, a SENSE reduction factor of five was consequently applied. Even though such high reduction factors are suboptimal in terms of SNR (36,37), smaller factors did not reduce the artifacts sufficiently in all subjects. The SNR drop was compensated by signal averaging so that the influence of the g-factor caused by the high SENSE reduction factor could be reduced.

Second, another problem interfering with the quality of data acquisition is the proximity of the supraclinoid segment of the internal carotid artery, which runs just

laterally to the optic nerve before dividing into the anterior and medial branches. Moreover, the ophthalmic artery follows the optic nerve through the optic canal. Pulsation of the carotid artery and its branches may induce motion artifacts in the anatomical area of the optic nerve, chiasm, and optic tract. Due to motion sensitivity of DTI, this may result in wrong directional diffusion tensor data (41,42), consequently leading to misdetection or even nondetection of fibers passing through this area. Therefore, cardiac gating was applied at two different time points to investigate pulsation effects. No differences in fiber reconstruction were detected within the two different cardiac gating time points used in this study. Additionally, the same results were achieved in datasets in which other cardiac time points were tested or in which cardiac gating even was omitted.

Third, resolving fiber crossing and branching situations with DTI based fiber tracking, such as, e.g., within the optic chiasm or the LGN, is a crucial problem. Newly developed tracking algorithms have to be applied that are designed especially for coping well with such situations.

A last important point for reliable fiber reconstruction was the angulation of the measurement slices. The angulation had to be defined according to the individual anatomical orientation of the optic chiasm, meaning that both optic nerves and both optic tracts as well as the chiasm should be visible in one slice. If they were not covered within one single slice, the aFM was not able to handle the fiber crossing correctly in the optic chiasm. A possible explanation is that an inadequate angulation augments partial volume effects, meaning that the data integrity in the area of the optic chiasm is compromised by surrounding tissues not belonging to the visual system. To reduce bulk motion for achieving accurate positioning of the imaging slices, it is important that the volunteers are well fixed inside the head coil with foam padding and do not move during and between the single scans. Another important point to reduce bulk motion was to shorten the total scan time as much as possible. The goal was to limit the overall time for the scan session to one hour. As a result, only nine DTI image slices could be acquired with the parameters defined in the data acquisition paragraph. Although the volume covered by these nine slices is relatively small, all parts of the visual system could be covered by exact angulation in the anterior brain regions (optic nerves, optic chiasm, optic tracts, and lateral geniculate nuclei). In the posterior area of the brain (optic radiation), where the fibers fan out to reach the visual cortex, it might be possible that not all parts of the visual system were covered. But, again, by an exact angulation, the main parts could be included in the imaging volume (see Figs. 4 and 5).

Previous publications showed fiber pathways in the region of the optic radiation (19,20,29) or parts of the optic nerve (27,28,46). To the authors' knowledge, until now, no DTI fiber tracking study was able to reconstruct the optic pathway in its entire length, and especially the fiber crossing in the optic chiasm. Regarding our results, which are all based on a single seed region approach, fibers reconstructed by the aFM algorithm are closely related to the corresponding anatomy. The aFM algorithm makes it possible to detect the entire fiber structure of the optic system from each of the three seed regions separately. Starting in the chiasm, it reconstructs the nerve fibers of the visual system in all four directions out of the chiasm, i.e., both optic nerves, the optic tracts, and the optic radiations up to the visual cortex. It should be noted that this branching behavior of the aFM algorithm could lead to wrong results in other crossing regions in which not all fiber outcomes are correct. If in such an area, e.g., only one pathway were correct, the aFM algorithm might probably fail. Furthermore, the fibers of the optic system reconstructed from the left or right optic nerve are consistent with physiological anatomical knowledge, meaning that one optic nerve divides into two hemiparts, which join contralateral fibers in the chiasm and follow the visual pathway on both sides into the visual cortex. Using the same data, we also tried to achieve similar results with the FACT algorithm (7), but an entire reconstruction, from the retina to the visual cortex, was not feasible from any of the three starting seed areas. Furthermore, it was not possible to resolve the fiber crossing situation within the optic chiasm.

Investigating the aFM-reconstructed fibers in more detail, filaments around the optic nerve, which fan out though the entire orbit in the direction of the eyeball, can be detected. This might be due to the embedding of the optic nerve between the eye muscles and the orbital fat. Other cranial nerves (III, IV, V_1, VI), though smaller in diameter than the optic nerve, are also found within the orbit. Thus, during the first phase of the aFM algorithm in which a three-dimensional wave front is expanded, the wave front may branch out and may include also voxels adjacent to the main fiber bundle, depending on the alignment of the underlying, local diffusion tensors and the result of the speed function evaluations. On one hand, this algorithmic feature gives the power to reconstruct fiber branching; on the other hand, it may be possible that the reconstructed fibers fan out in some areas.

Reconstructed fiber bundles emerging from the chiasm in straight posterior direction (in direction of the brain stem) may represent the oculomotor nerves (III. cranial nerve) to their nuclei in the brain stem. Filaments on both sides that diverge in posterior direction from the optic radiation may represent connections to higher order visual fields or fibers of the corticotectal tract and the posterior thalamic radiation. These fiber pathways are also described in publications by Parker (19) and Ciccarelli et al (29), whereas other studies did not show these interconnections (e.g., (23,47)).

An important point when performing DTI fiber tracking is the reproducibility of the reconstructed tracks. In this study, intersubject and intrasubject reproducibility (by measuring four subjects at two different days and reconstructing fibers from the three seed areas in the different datasets of the same subject) were tested to approve the anatomically accurate reconstruction of the specific fiber pathways. The reconstructed fibers visible in Figs. 4 and 5 for two different subjects and two different cardiac gating time points, as well as the fibers

reconstructed in all other subjects, look very similar to each other.

In conclusion, the results presented in this study demonstrate that the choice of an accurate tracking algorithm is a decisive point for the reconstruction of fiber tracks in the human brain. The results illustrate that the aFM algorithm handles the fiber crossing within the optic chiasm correctly and provides results that are in good agreement with anatomical knowledge. Nevertheless, when performing fiber tracking and interpreting tracking results, one should be aware of the limitations of DTI-based fiber tracking itself and the applied algorithm. A critical verification, such as, e.g., comparing the results to known anatomy, is inalienable.

REFERENCES

1. Basser PJ, Mattiello J, LeBihan D. MR diffusion tensor spectroscopy and imaging. Biophys J 1994;66:259–267.
2. Pierpaoli C, Jezzard P, Basser PJ, Barnett A, Di Chiro G. Diffusion tensor MR imaging of the human brain. Radiology 1996;201:637–648.
3. Poupon C, Clark CA, Frouin V, Bloch I, Le Bihan D, Mangin JF. Tracking white matter fascicles with diffusion tensor imaging. In: Proceedings of the 7th Annual Meeting of ISMRM, Philadelphia, PA, USA, 1999 (Abstract 325).
4. Lori NF, Cull TS, Akbudak E, et al. Tracking neuronal fibers in the living human brain with diffusion MRI. In: Proceedings of the 7th Annual Meeting of ISMRM, Philadelphia, PA, USA, 1999 (Abstract 324).
5. Mori S, Crain BJ, Chacko VP, van Zijl PC. Three-dimensional tracking of axonal projections in the brain by magnetic resonance imaging. Ann Neurol 1999;45:265–269.
6. Bammer R, Acar B, Moseley ME. In vivo MR tractography using diffusion imaging. Eur J Radiol 2003;45:223–234.
7. Mori S, van Zijl PC. Fiber tracking: principles and strategies—a technical review. NMR Biomed 2002;15:468–480.
8. Basser PJ, Pajevic S. Statistical artifacts in diffusion tensor MRI (DT-MRI) caused by background noise. Magn Reson Med 2000;44:41–50.
9. Lazar M, Alexander AL. An error analysis of white matter tractography methods: synthetic diffusion tensor field simulations. Neuroimage 2003;20:1140–1153.
10. Lazar M, Alexander AL. Bootstrap white matter tractography (BOOT-TRAC). Neuroimage 2005;24:524–532.
11. Tournier JD, Calamante F, King MD, Gadian DG, Connelly A. Limitations and requirements of diffusion tensor fiber tracking: an assessment using simulations. Magn Reson Med 2002;47:701–708.
12. Watts R, Liston C, Niogi S, Ulug AM. Fiber tracking using magnetic resonance diffusion tensor imaging and its applications to human brain development. Ment Retard Dev Disabil Res Rev 2003;9:168–177.
13. Jones DK, Basser PJ. "Squashing peanuts and smashing pumpkins": how noise distorts diffusion-weighted MR data. Magn Reson Med 2004;52:979–993.
14. Jones DK. Determining and visualizing uncertainty in estimates of fiber orientation from diffusion tensor MRI. Magn Reson Med 2003;49:7–12.
15. Lazar M, Weinstein DM, Tsuruda JS, et al. White matter tractography using diffusion tensor deflection. Hum Brain Mapp 2003;18:306–321.
16. Weinstein D, Kindlmann G, Lundberg E. Tensorlines: Advection-diffusion based propagation through diffusion tensor fields. IEEE Visualisation 1999 (Proceedings of the conference on Visualization '99: celebrating ten years):249–253.
17. Westin CF, Maier SE, Mamata H, Nabavi A, Jolesz FA, Kikinis R. Processing and visualization for diffusion tensor MRI. Med Image Anal 2002;6:93–108.
18. Zhang S, Bastin ME, Laidlaw DH, Sinha S, Armitage PA, Deisboeck TS. Visualization and analysis of white matter structural asymmetry in diffusion tensor MRI data. Magn Reson Med 2004;51:140–147.
19. Parker GJM, Wheeler-Kingshott CAM, Barker GJ. Estimating distributed anatomical connectivity using fast marching methods and diffusion tensor imaging. IEEE Trans Med Imaging 2002;21:505–512.
20. Staempfli P, Jaermann T, Crelier GR, Kollias S, Valavanis A, Boesiger P. Resolving fiber crossing using advanced fast marching tractography based on diffusion tensor imaging. Neuroimage 2006;30:110–120.
21. Rademacher J, Burgel U, Zilles K. Stereotaxic localization, intersubject variability, and interhemispheric differences of the human auditory thalamocortical system. Neuroimage 2002;17:142–160.
22. Rademacher J, Burgel U, Geyer S, et al. Variability and asymmetry in the human precentral motor system. A cytoarchitectonic and myeloarchitectonic brain mapping study. Brain 2001;124(Pt 11):2232–2258.
23. Burgel U, Amunts K, Hoemke L, Mohlberg H, Gilsbach JM, Zilles K. White matter fiber tracts of the human brain: three-dimensional mapping at microscopic resolution, topography and intersubject variability. Neuroimage 2006;29:1092–1105.
24. Burgel U, Schormann T, Schleicher A, Zilles K. Mapping of histologically identified long fiber tracts in human cerebral hemispheres to the MRI volume of a reference brain: position and spatial variability of the optic radiation. Neuroimage 1999;10:489–499.
25. Mori S, Wakana S, van Zijl PCM, Nagae-Poetscher LM. MRI atlas of human white matter. Elsevier; 2005. p 276.
26. Wakana S, Jiang H, Nagae-Poetscher LM, van Zijl PC, Mori S. Fiber tract-based atlas of human white matter anatomy. Radiology 2004;230:77–87.
27. Trip SA, Wheeler-Kingshott C, Jones SJ, et al. Optic nerve diffusion tensor imaging in optic neuritis. Neuroimage 2005.
28. Iwasawa T, Matoba H, Ogi A, et al. Diffusion-weighted imaging of the human optic nerve: a new approach to evaluate optic neuritis in multiple sclerosis. Magn Reson Med 1997;38:484–491.
29. Ciccarelli O, Toosy AT, Hickman SJ, et al. Optic radiation changes after optic neuritis detected by tractography-based group mapping. Hum Brain Mapp 2005;25:308–316.
30. Schoth F, Burgel U, Dorsch R, Reinges MH, Krings T. Diffusion tensor imaging in acquired blind humans. Neurosci Lett 2006.
31. Vinogradov E, Degenhardt A, Smith D, et al. High-resolution anatomic, diffusion tensor, and magnetization transfer magnetic resonance imaging of the optic chiasm at 3T. J Magn Reson Imaging 2005;22:302–306.
32. Standring S. Gray's anatomy. Churchill Livingstone; 2005.
33. Waldeyer A, Mayet A. Anatomie des Menschen 1 und 2. de Gruyter; 1993.
34. Batchelor PG, Atkinson D, Hill DL, Calamante F, Connelly A. Anisotropic noise propagation in diffusion tensor MRI sampling schemes. Magn Reson Med 2003;49:1143–1151.
35. Bammer R, Auer M, Keeling SL, et al. Diffusion tensor imaging using single-shot SENSE-EPI. Magn Reson Med 2002;48:128–136.
36. Jaermann T, Crelier G, Pruessmann KP, et al. SENSE-DTI at 3 T. Magn Reson Med 2004;51:230–236.
37. Jaermann T, Pruessmann KP, Valavanis A, Kollias S, Boesiger P. Influence of SENSE on image properties in high-resolution single-shot echo-planar DTI. Magn Reson Med 2006;55:335–342.
38. Pruessmann KP, Weiger M, Scheidegger MB, Boesiger P. SENSE: sensitivity encoding for fast MRI. Magn Reson Med 1999;42:952–962.
39. Poncelet BP, Wedeen VJ, Weisskoff RM, Cohen MS. Brain parenchyma motion: measurement with cine echo-planar MR imaging. Radiology 1992;185:645–651.
40. Greitz D, Wirestam R, Franck A, Nordell B, Thomsen C, Stahlberg F. Pulsatile brain movement and associated hydrodynamics studied by magnetic resonance phase imaging. The Monro-Kellie doctrine revisited. Neuroradiology 1992;34:370–380.
41. Jones DK, Pierpaoli C. Contribution of cardiac pulsation to variability of tracking results. In: Proceedings of the 13th Annual Meeting of ISMRM, Miami Beach, FL, USA, 2005 (Abstract 222).
42. Pierpaoli C, Marenco S, Rohde G, Jones DK, Barnett AS. Analyzing the contribution of cardiac pulsation to the variability of quantities derived from the diffusion tensor. In: Proceedings of the 11th Annual Meeting of ISMRM, Toronto, Ontario, Canada, 2003 (Abstract 70).

43. Netsch T, vanMuiswinkel A. Quantitative evaluation of image-based distortion correction in diffusion tensor imaging. IEEE Trans Med Imaging 2004;23:789–798.
44. Parker GJ, Stephan KE, Barker GJ, et al. Initial demonstration of in vivo tracing of axonal projections in the macaque brain and comparison with the human brain using diffusion tensor imaging and fast marching tractography. Neuroimage 2002;15:797–809.
45. Westin CF, Peled S, Gudbjartsson H, Kikinis R, Jolesz FA. Geometrical diffusion measures for MRI from tensor basis analysis. In: Proceedings of the 5th Annual Meeting of ISMRM, Vancouver, British Columbia, Canada, 1997 (Abstract 1742).
46. Chabert S, Molko N, Cointepas Y, Le Roux P, Le Bihan D. Diffusion tensor imaging of the human optic nerve using a non-CPMG fast spin echo sequence. J Magn Reson Imaging 2005;22:307–310.
47. Kang N, Zhang J, Carlson ES, Gembris D. White matter fiber tractography via anisotropic diffusion simulation in the human brain. IEEE Trans Med Imaging 2005;24:1127–1137.